Precursor to the Onset of the Bulk Oxidation of Cu(100)

Liang Li,[1] Xi Mi,[2] Yunfeng Shi,[2] and Guangwen Zhou[1,*]

[1]*Department of Mechanical Engineering & Multidisciplinary Program in Materials Science and Engineering, State University of New York, Binghamton, New York 13902, USA*

[2]*Department of Materials Science and Engineering, Rensselaer Polytechnic Institute, Troy, New York 12180, USA*

(Received 27 March 2011; revised manuscript received 10 October 2011; published 26 April 2012)

Using density-functional theory within the generalized gradient approximation, we investigate the energetics of oxygen subsurface adsorption governing the onset of bulk oxidation of Cu(100) surface. It shows that the presence of boundaries formed from merged missing-row nanodomains mismatched by a half unit-cell leads to preferred oxygen adsorption at the subsurface tetrahedral sites. The resulting Cu-O tetrahedrons along the domain boundary strikingly resemble that of the bulk oxide phase of Cu_2O. These results provide direct atomic-scale insight into the microscopic origin of the crystallographic orientation relationships for oxide overlayer growth. Our results also suggest that the oxidation of an atomically flat terrace can still be a heterogeneous nucleation process controlled by defects in the oxygen-chemisorbed adlayer.

DOI: 10.1103/PhysRevLett.108.176101 PACS numbers: 68.43.Bc, 68.43.Fg, 68.47.De

The oxidation of metals is a universal reaction caused by the simple fact that the oxide of most metals is more stable than the metal itself. Upon exposure to an oxygen atmosphere, the metal surface undergoes a series of structure changes from the initial oxygen chemisorption to oxygen diffusion into the subsurface region and then to bulk oxide formation. While considerable progress has been made in understanding the behavior of oxygen chemisorption, it has been focused mostly on solving the atomic structure of oxygen-chemisorbed layers. The effect of oxygen chemisorption on bulk oxide formation is still to a significant degree unclear. In particular, the atomic details of oxygen-adsorption induced transformation of the metal crystal lattice into its oxide are not resolved.

The oxidation of copper has been a rich source of information to understand the corrosion of metals [1–16]. The initial oxidation of Cu(100) typically goes through several reconstructions: for oxygen coverage below 0.3 monolayer (ML), oxygen adsorbs on fourfold hollow sites resulting in a Cu(100) $-$ $c(2 \times 2)$ structure [1–3]. Increased oxygen exposure induces nucleation of $(2\sqrt{2} \times \sqrt{2})R45°$ missing-row domains that grow and merge with a saturated oxygen coverage of 0.5 ML [2–5,14,17]. Further oxygen adsorption leads to Cu_2O formation [6,7,18–20], initialized by oxygen embedment into Cu subsurface region [8,10,15,21].

In FCC (face-cubic centered) Cu lattice, two types of interstitial sites, i.e., octahedral and tetrahedral sites, are available for possible subsurface oxygen occupancy. Density-functional theory (DFT) calculations showed that the octahedral site is more favorable than the tetrahedral site for oxygen adsorption [9–11,15,16]. This is in contrast with Cu_2O structure in which oxygen has to reside the tetrahedral sites $(\frac{1}{4}, \frac{1}{4}, \frac{1}{4})$ and $(\frac{3}{4}, \frac{3}{4}, \frac{3}{4})$ of FCC Cu lattice (Fig. 1). Therefore, oxygen octahedral site occupancy is not an indication of Cu_2O nucleation. Here we show that the presence of domain boundaries formed by merged $(2\sqrt{2} \times \sqrt{2})R45° - O$ nanodomains indeed results in preferred oxygen adsorption at the tetrahedral sites and the bond length or angle and electron charge transfer of the Cu-O tetrahedron resembles closely that of the Cu_2O structure. Surface defects such as steps are generally agreed to be the preferential sites for oxide nucleation. However, the mechanism governing oxide nucleation on flat surface terraces has been a matter of longstanding debate [22–24]. Our results indicate that even for an atomically flat surface the oxide nucleation can be still a heterogeneous process limited by defects in the oxygen-chemisorbed layer.

The surface restructuring by oxygen chemisorption shows a two-dimensional nucleation and growth mechanism, which results in reconstructed nanodomains along

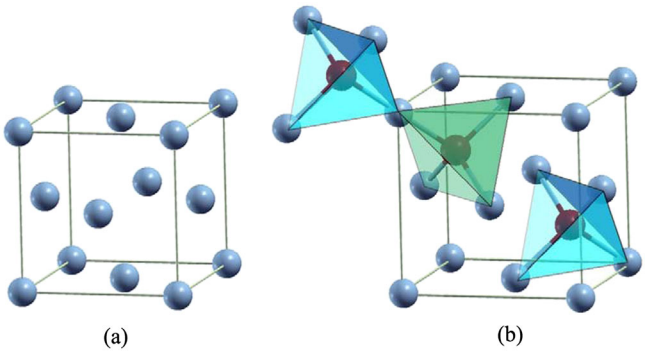

FIG. 1 (color online). The comparison of FCC structure of Cu (a) to the cubic structure of Cu_2O (b) Oxygen atoms have to reside the tetrahedral sites to form Cu_2O structure, where the tetrahedrons inside and adjacent to the cubic cell are highlighted. Blue and red balls represent Cu and O atoms, respectively.

with a high density of domain boundaries [1,5,7,8,17,25]. For Cu(100)- $(2\sqrt{2} \times \sqrt{2})R45° - O$ restructuring, where every fourth row of Cu atoms is missing, six domain boundaries can develop, depending on the orientations (parallel or perpendicular) of the missing rows: For boundaries formed by parallel missing rows, two types of boundaries can develop, one by 1/2 unit-cell mismatch between missing rows [Fig. 2(a)] and the other by 1 unit-cell mismatch [Fig. 2(b)]; For boundaries formed by perpendicular missing rows, four boundaries can develop, classified by the distance between the domain boundary to its nearest [100] missing row, which can be 1/2 unit-cell length [Fig. 2(c)], 1 unit-cell length [Fig. 2(d)], 3/2 unit-cell length [Fig. 2(e)], and 2 unit-cell length [Fig. 2(f)]. We use DFT to examine the subsurface oxygen adsorption at these boundaries. All the calculations are performed using the PWscf package with generalized gradient approximation and ultrasoft pseudo potentials [26,27].

Six supercells are constructed for the different boundaries, as illustrated in Fig. 3. Supercells with two boundaries are constructed for all the boundaries. It is crucial to include enough space between the two boundaries in the supercell to preclude any appreciable boundary-boundary interaction. To ensure the accuracy of comparison, supercells with the same size are adopted. The bulk lattice constants for Cu and Cu_2O are determined to be 3.64 Å and 4.30 Å, respectively. An energy cutoff of 27 Ry for the plane wave expansion is used. Five atomic layers are used for all the simulation cells, with the bottom two layers fixed while the rest are allowed to relax fully in all three dimensions until force components acting on each atom is lower than 0.001 Ry/Bohr (0.025 eV/Å). Adjacent slabs are separated by a 12 Å vacuum region. The calculation for the oxygen molecule is spin polarized. The Brillouin zone is sampled using a Monkhorst-Pack mesh using the special-point Gaussian smearing technique, with a smearing parameter of 0.03 Ry [28]. An $8 \times 2 \times 1$ mesh is used for all the supercells. We also compared the energies of subsurface oxygen adsorption in the middle of the boundary cells (an adsorption site equidistant from the two boundaries) with the perfect missing-row supercell. Their resulting energy differences are less than 0.015 eV, confirming that the effect of boundary-boundary interaction is negligible for the constructed supercells.

We first compared the interstitial sites in the region away from the boundaries with those of the perfect missing-row structure and a similar behavior is noted; i.e., the octahedral sites are preferred over the tetrahedral sites for oxygen subsurface adsorption. This thus allows us to focus on the subsurface sites associated with the boundaries. As seen in Fig. 3, there are two sets of interstitial sites associated with the boundaries, i.e., one alongside the missing row and the other having one atom row away from the missing row. The missing row has been shown to be the preferred diffusion path for oxygen embedment [9], suggesting interstitial sites alongside the missing row are kinetically more favorable for oxide nucleation. In Fig. 3, all the nonequivalent tetrahedral and octahedral sites alongside the missing row are identified.

A Cu double row is formed at the boundary for Parallel-I boundary [Fig. 2(a)]. We first check the preferential adsorption site between the two on-surface hollow sites, H1 and H2 (see the zoomed-in inset of Fig. 3(b)], within the Cu double row and subsurface sites for an additional oxygen atom. We find that the oxygen-adsorption energy for H1 site is −1.23 eV, lower than that for other sites. Further comparison shows that the oxygen surface adsorption energy for H2 site is ~0.4 eV and ~0.1 eV higher than $T2$ and $T5$ sites, respectively. Therefore, oxygen first adsorbs on H1 site resulting in 0.5 ML coverage [Fig. 3(b)].

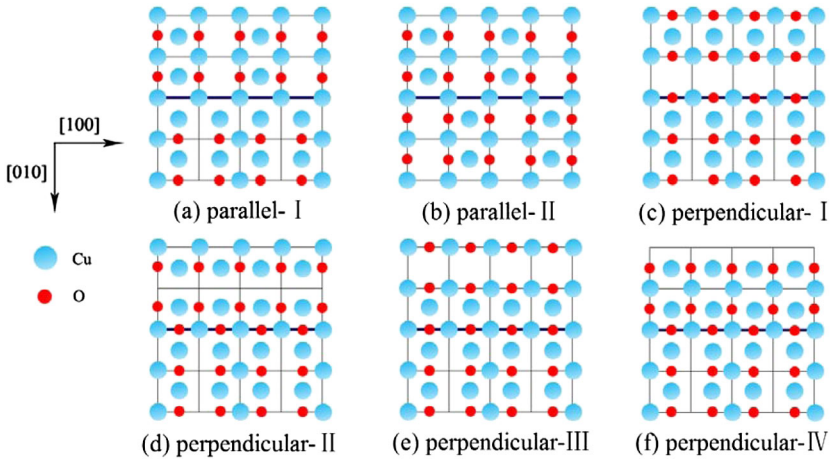

FIG. 2 (color online). Boundaries formed by merged Cu(100)-$(2\sqrt{2} \times \sqrt{2})R45° - O$ domains induced by oxygen surface chemisorption: (a) parallel missing rows with half unit-cell mismatch; (b) parallel missing rows with one-unit-cell missing-row mismatch; (c),(d),(e), and (f) boundaries formed by perpendicular missing rows with 1/2, 1, 3/2, and 2 unit-cell distance between the domain boundary and the nearest 100 missing row, respectively. Note that the unit cell is defined by the conventional cell (FCC) of Cu lattice.

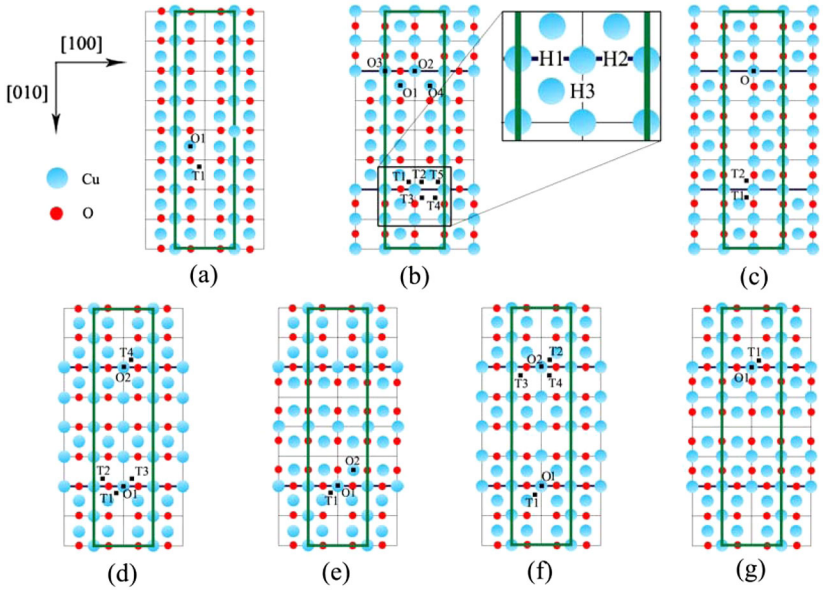

FIG. 3 (color online). The supercells used in our DFT calculations: (a) perfect missing-row structure, no domain boundary present, (b) Parallel-I boundary, H1 is a fully-coordinated on-surface hollow site, H2 and H3 are three-coordinated on-surface hollow sites (see zoomed-in inset); (c) Parallel-II boundary; (d) Perpendicular-I boundary; (e) Perpendicular-II boundary; (f) Perpendicular-III boundary; and (g) Perpendicular-IV boundary. Note that the perpendicular missing-row domains with $1/2$ and $3/2$ unit-cell distances result in the same supercells with only 180° rotation (i.e., d and f) for maintaining the same cell size.

At the oxygen coverage of 0.53 ML with one subsurface oxygen, the calculation results show that the subsurface tetrahedral oxygen (STO) at $T2$ and $T5$ sites have adsorption energy of -1.10 eV and -0.84 eV, respectively, significantly lower than all other subsurface sites.

The oxygen subsurface adsorption for the perfect missing-row structure and other boundaries is also examined (Table I). It can be seen that the octahedral sites are more favored for oxygen to occupy for the perfect missing-row structure and Parallel-II and Perpendicular-I, III boundaries. Perpendicular-II [Fig. 2(d)] and IV [Fig. 2(f)] boundaries have more dense oxygen packing along the boundaries, and the corresponding supercells [Figs. 3(e) and 3(g)] have the oxygen coverage of 0.59 ML with one subsurface oxygen. Note that their deviation from the 0.5 ML coverage is due to the small domain size (or significant boundary presence). As the supercell size becomes larger, the oxygen coverage approaches to the expected 0.5 ML value. The DFT results show that the oxygen-adsorption energies for both the octahedral and tetrahedral sites associated with these two boundaries have positive values, making them unstable for oxygen adsorption.

The above results reveal that the subsurface oxygen-adsorption energies can be changed appreciably by presence of the boundaries. Their comparison in Table I shows evidently that only Parallel-I boundary results in preferred oxygen adsorption at the tetrahedral sites. Since nucleating Cu_2O on Cu(100) surface requires oxygen to reside in tetrahedral sites, the significant reduction in the adsorption energy of oxygen at Parallel-I boundary suggests its preference for Cu_2O nucleation.

TABLE I. The energies (eV) for oxygen adsorption at the subsurface interstitial sites alongside the missing rows of the different surface regions.

	STO (tetrahedral site)					SOO (octahedral site)				Oxygen coverage (ML)
	$T1$	$T2$	$T3$	$T4$	$T5$	O1	O2	O3	O4	
$(2\sqrt{2}\times\sqrt{2})R45°$ − O (no boundary)	−0.36					−0.47				0.53
Parallel-I boundary	−0.21	−1.10	−0.27	−0.29	−0.84	−0.29	−0.13	−0.11	−0.14	0.53
Parallel-II boundary	−0.18	−0.40				−0.57				0.53
Perpendicular-I boundary	−0.38	−0.31	−0.28	−0.35		−0.47	−0.56			0.53
Perpendicular-II boundary	0.17					0.11	0.09			0.59
Perpendicular-III boundary	−0.35	−0.38	−0.31	−0.28		−0.56	−0.47			0.53
Perpendicular-IV boundary	0.19					0.13				0.59

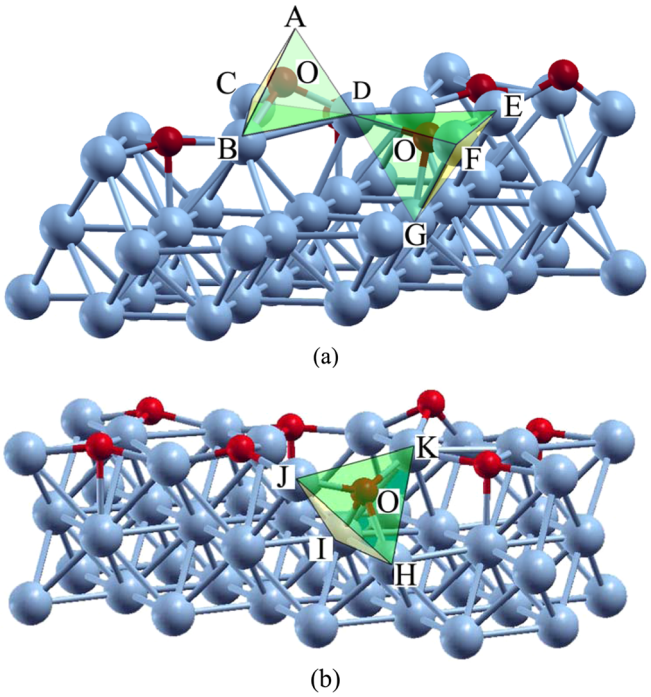

FIG. 4 (color online). Equilibrium structure of the STOs formed from oxygen subsurface adsorption at (a) $T2$ and (b) $T5$ sites along with Parallel-I boundary, the resulting tetrahedrons are highlighted.

Because the oxygen occupancy at the tetrahedral T2 and $T5$ sites along Parallel-I boundary resembles Cu_2O, we thus examine more closely the equilibrium structures of tetrahedral oxygen at these sites. As seen in Fig. 4(a), the fully relaxed structure shows that the STO at T2 shifts slightly upwards with accompanying displacement of on-surface Cu atoms, resulting in a Cu-O tetrahedron (the tetrahedron DEFG). In addition, the on-surface oxygen which initially sits on the on-surface hollow site [H3 site shown in the zoomed-in inset of Fig. 3(b)] is pushed outward, resulting in another Cu-O tetrahedron with the coordinating Cu atoms B, C, and D (note in this tetrahedron there is no Cu atom available at the top corner A). The two tetrahedrons are corner-sharing, resulting in a linear O-Cu-O chain structure, as seen in Cu_2O structure [Fig. 1(b)]. The measured O-O distance and bond angle of this O-Cu-O chain is 3.64 Å and 171.3°, and the corresponding values for Cu_2O structure are 3.72 Å and 180°, respectively. By comparing with Fig. 1(b), it can be also seen that the on-surface Cu atoms (B-C-D-E-F) of the two corner-sharing Cu-O tetrahedrons corresponds to $Cu_2O(111)$ plane. Thus, the epitaxial relation for Cu_2O nucleation observed here is $Cu_2O(111)//Cu(100)$, which has been observed experimentally [29]. The fully relaxed structure of the STO at $T5$ is illustrated in Fig. 4(b), where the Cu-O tetrahedron is labeled by HIJK. The obtained bond lengths and bond angles of the Cu-O tetrahedrons are compared with those of the Cu-O tetrahedron in Cu_2O structure and show striking resemblance (Table II). However, unlike the $T2$ site, oxygen adsorption at $T5$ does not cause significant atom displacement and the STO is still stabilized at the $T5$ site. This results in the epitaxial relationship of $Cu_2O(100)//Cu(100)$, which has been also observed experimentally [30].

To understand why presence of Parallel-I boundary results in preferred oxygen adsorption at the tetrahedral $T2$ and $T5$ sites, we first examine the bond lengths of the STO and SOO for Parallel-I boundary. The oxygen subsurface adsorption is induced by the significant O-O repulsion that arises as the oxygen surface coverage increases [9,11,13,31]. The formation of strong and shorter Cu-O bond can effectively screen the increasing O-O repulsion [11]. Our calculations indicate that the distances from STO or SOO to the on-surface oxygen are similar (~ 3.67 Å); however, in the STO tetrahedrons induced by oxygen adsorption at $T2$ and $T5$ sites, the average Cu-O bond length is ~1.90 Å (Table II), whereas for the stable SOO structure, the average Cu-O bond length is 2.10 Å. The shorter Cu-O bond lengths in the STO tetrahedron promote its oxygen adsorption. A Löwdin population analysis reveals that the distribution of valence electrons of the STOs at Parallel-I boundary $T2$ and $T5$ sites is $s^{1.85}p^{5.19}$, $s^{1.82}p^{5.26}$ and $s^{1.86}p^{5.23}$, which indicates that the oxygen ions gain 1.04, 1.08, and 1.09 electrons, respectively, in the three Cu-O tetrahedrons. This is in accordance with the reported effective charge of (0.9-1.3) for oxygen in the

TABLE II. Comparison of the bond lengths and angles determined from the three tetrahedrons resulting from oxygen adsorption at $T2$ and $T5$ of Parallel-I boundary to the corresponding Cu-O tetrahedron in Cu_2O

	Bond length (Å)				Average Cu-O-Cu bond angle (°)
On-surface Cu-O tetrahedron resulting from O adsorption at $T2$	1.90 (OB)	1.85 (OC)	1.80 (OD)		97.37
Subsurface Cu-O tetrahedron resulting from O adsorption at $T2$	1.84 (OD)	1.84 (OE)	1.90 (OF)	2.00 (OG)	107.93
Subsurface Cu-O tetrahedron resulting from O adsorption at $T5$	1.94 (OH)	2.03 (OI)	1.96 (OJ)	1.85 (OK)	106.56
Cu-O tetrahedron in Cu_2O	1.86	1.86	1.86	1.86	109.47

Cu_2O structure [32]. It should be noted that, due to surface effect and under-coordination, the electron transfer per Cu to O in the incomplete tetrahedron (ABCD) is more than the complete tetrahedron by ~25%.

The preferred oxygen adsorption at the tetrahedral *T*2 and *T*5 sites of Parallel-I boundary is also facilitated by its increased Cu coordination. As noted in Fig. 3, the STO of the perfect missing-row structure has three coordinating Cu atoms, one on-surface Cu atom, and two second-layer Cu atoms (not shown in the figure), whereas the STO of Parallel-I boundary *T*2 and *T*5 sites has four nearest Cu atoms. Their increased Cu coordination promotes the oxygen occupancy. Although Parallel-I boundary *T*1 site (and similar *T*1 sites for other boundaries) also has four coordinating Cu atoms, the repulsion force from the adjacent on-surface oxygen makes this type of sites unfavorable for oxygen adsorption. Such effect is even more pronounced for Perpendicular-II and IV boundaries, where the strong repulsion force from the closely packed on-surface oxygen makes both the tetrahedral and octahedral sites unsuitable for oxygen adsorption. We then compare the subsurface sites for other boundaries. Although some STOs (i.e., *T*1 sites for Parallel-II and Perpendicular-I, III boundaries) have 4 nearest Cu atoms, the SOOs of these boundaries have higher symmetrical bonding with on-surface oxygen atoms, which effectively balances the O-O repulsion and thus make these SOOs more stable than their STO counterparts.

In summary, we have examined the energetics of oxygen subsurface adsorption during the oxidation of Cu(100). Our results demonstrate that the oxidation of Cu(100) terrace is via a heterogeneous nucleation process, where the boundaries formed by merged parallel missing-row domains with half unit-cell mismatch are preferred sites for forming Cu_2O-type Cu-O tetrahedrons with the orientation relationships of $Cu_2O(111)//Cu(100)$ and $Cu_2O(100)//Cu(100)$. The approach obtained from this study can be extended to understand the transient oxidation of other metals, where oxygen-chemisorption induced surface restructuring generally occurs, but its effect on initiating the onset of the bulk oxide formation has hitherto rarely been addressed.

We thank Vincent Meunier for fruitful discussion on this work. Research supported by the U.S. Department of Energy, Office of Basic Energy Sciences, Division of Materials Sciences and Engineering under Grant No. DE-FG02-09ER46600. This work used the Extreme Science and Engineering Discovery Environment.

*To whom correspondence should be addressed.
gzhou@binghamton.edu

[1] T. Fujita, Y. Okawa, Y. Matsumoto, and K. I. Tanaka, Phys. Rev. B **54**, 2167 (1996).
[2] H. Iddir, D. D. Fong, P. Zapol, P. H. Fuoss, L. A. Curtiss, G. W. Zhou, and J. A. Eastman, Phys. Rev. B **76**, 241404 (R) (2007).
[3] M. Kittel, M. Polcik, R. Terborg, J. T. Hoeft, P. Baumgartel, A. M. Bradshaw, R. L. Toomes, J. H. Kang, D. P. Woodruff, M. Pascal, C. L. A. Lamont, and E. Rotenberg, Surf. Sci. **470**, 311 (2001).
[4] I. K. Robinson, E. Vlieg, and S. Ferrer, Phys. Rev. B **42**, 6954 (1990).
[5] F. Besenbacher and J. K. Norskov, Prog. Surf. Sci. **44**, 5 (1993).
[6] J. A. Eastman, P. H. Fuoss, L. E. Rehn, P. M. Baldo, G. W. Zhou, D. D. Fong, and L. J. Thompson, Appl. Phys. Lett. **87**, 051914 (2005).
[7] M. Lampimaki, K. Lahtonen, M. Hirsimaki, and M. Valden, J. Chem. Phys. **126**, 034703 (2007).
[8] K. Lahtonen, M. Hirsimaki, M. Lampimaki, and M. Valden, J. Chem. Phys. **129**, 124703 (2008).
[9] M. Y. Lee and A. J. H. McGaughey, Surf. Sci. **603**, 3404 (2009).
[10] M. Y. Lee and A. J. H. McGaughey, Surf. Sci. **604**, 1425 (2010).
[11] X. Duan, O. Warschkow, A. Soon, B. Delley, and C. Stampfl, Phys. Rev. B **81**, 075430 (2010).
[12] A. Soon, M. Todorova, B. Delley, and C. Stampfl, Surf. Sci. **601**, 5809 (2007).
[13] A. Soon, M. Todorova, B. Delley, and C. Stampfl, Phys. Rev. B **73**, 165424 (2006).
[14] K. W. Jacobsen and J. K. Nłrskov, Phys. Rev. Lett. **65**, 1788 (1990).
[15] T. Kangas and K. Laasonen, Surf. Sci. **602**, 3239 (2008).
[16] T. Kangas, K. Lassonen, A. Puisto, H. Pitkanen, and M. Alatalo, Surf. Sci. **584**, 62 (2005).
[17] F. Jensen, F. Besenbacher, E. Laegsgaard, and I. Stensgaard, Phys. Rev. B **42**, 9206 (1990).
[18] J. C. Yang, D. Evan, and L. Tropia, Appl. Phys. Lett. **81**, 241 (2002).
[19] G. W. Zhou and J. C. Yang, Surf. Sci. **531**, 359 (2003).
[20] G. W. Zhou, Phys. Rev. B **81**, 195440 (2010).
[21] K. R. Lawless, Rep. Prog. Phys. **37**, 231 (1974).
[22] D. F. Mitchell, P. B. Sewell, and M. Cohen, Surf. Sci. **61**, 355 (1976).
[23] P. H. Holloway, J. Vac. Sci. Technol. **18**, 653 (1981).
[24] E. Kopatzki and R. J. Behm, Phys. Rev. Lett. **74**, 1399 (1995).
[25] F. Besenbacher, Rep. Prog. Phys. **59**, 1737 (1996).
[26] J. P. Perdew, K. Burke, and M. Ernzerhof, Phys. Rev. Lett. **77**, 3865 (1996).
[27] P. Giannozzi *et al.*, J. Phys. Condens. Matter **21**, 395502 (2009).
[28] H. J. Monkhorst and J. D. Pack, Phys. Rev. B **13**, 5188 (1976).
[29] C. L. H. Devlin, Y. Sato, and S. Chiang, J. Appl. Phys. **105**, 123534 (2009).
[30] G. W. Zhou and J. C. Yang, Phys. Rev. Lett. **89**, 106101 (2002).
[31] S. Jaatinen, J. Blomqvist, P. Salo, A. Puisto, M. Alatalo, M. Hirsimaki, M. Ahonen, and M. Valden, Phys. Rev. B **75**, 075402 (2007).
[32] S.-G. Wang and W. H. Eugen Schwarz, Angew. Chem., Int. Ed. **39**, 1757 (2000).